Monitoring of scale formation in a pneumatic conveying system operating in a metal production plant

Ingrid Bokn Haugland [a,b,*], Jana Chladek [a], Maths Halstensen [b]

[a] SINTEF Tel-Tek, SINTEF Industry, Kjølnes ring 30, N-3918 Porsgrunn, Norway
[b] Faculty of Technology, Natural Sciences and Maritime Sciences, University of South-Eastern Norway, P.O Box 203, N-3901 Porsgrunn, Norway

ABSTRACT

Monitoring of scale progression in a pneumatic conveying system operating in a metal production plant was conducted during a five-month long monitoring period. A combination of an acoustic monitoring method and a laser imaging method provided detailed information of gradual scale growth in a test pipe. The results show that the scale grew steadily throughout the test campaign. Periods of increasing and decreasing scale growth rate as well as episodes where the scale was detached from the pipe surface could be identified. Additionally, visual inspection of images obtained by the laser device offered information about the spatial distribution of the scale in a cross section of the test pipe.
This is an open access article under the CC BY-NC-ND license. (http://creativecommons.org/licenses/by-nc-nd/4.0/).

1. Introduction

Pneumatic conveying is widely used to transport powder materials in many industries due to its many advantages such as flexibility in pipeline layout with possibility of several pick-up and delivery points, easy automation and fully enclosed transportation enabling dust-free transfer of materials [1]. Although the theoretical understanding of dense phase conveying is not as complete as for dilute phase, dense phase conveying is often the preferred option because of low energy cost and low wear [2]. In dense phase conveying, powder is transported with lower gas velocities and thereby, wear of equipment and particle attrition can be reduced. Furthermore, longer transportation distances become feasible and increased material throughput can be achieved with additional rewards of lower energy consumption and lower cost of operation [1,3]. However, some challenges with potential to hamper both dilute and dense phase pneumatic conveying systems remain. One such challenge is the deposition of unwanted material, also referred to as scale formation, in pipelines.

Deposition of a material called hard grey scale (HGS) on process equipment is a considerable issue in aluminium production plants [4]. In such plants, powdered alumina is used as a sorbent in dry scrubbing systems, adsorbing fluorides and other compounds from the production off-gases and thus forming secondary alumina [5]. Subsequently, it is used as a raw material in the aluminium production process. HGS deposits in the distribution systems for secondary alumina, particularly

in pneumatic conveying lines transporting the material to metal production pots. Scale formation interferes with the operation of the conveying systems, resulting in both the need for cleaning and maintenance of the equipment, but also operational down time [4]. The formation mechanism of alumina scale is assumed to be complex and depending on several factors such as moisture, temperature and the composition of the process off-gas. Additionally, chemical reactions of compounds adsorbed on alumina in the dry scrubbing process may be involved. Scaling is also found to be more severe in high-turbulent areas along the secondary alumina transportation path. Some possible formation mechanisms have been suggested in the literature [4,6], but no final conclusion explaining the scaling issue has been reached.

Process analytical technology (PAT) is an emerging field focusing on monitoring of critical process parameters and quality attributes in industrial applications using advanced sensor technology and data analysis methods [7]. Acoustic chemometrics is a non-invasive, real-time PAT technique [8]. In a recent study, a new, active version of the acoustic monitoring technique was presented. Feasibility tests of the active acoustic method suggested that it can be used for monitoring of scaling in pneumatic conveying systems. However, a challenge of the method is that it relies on model calibration against reliable reference measurements of scale growth. Also, the method is sensitive to specific physical properties of the monitored system. Thus, on site calibration is necessary [9]. To solve this issue, a technique for obtaining reference measurements of scale depositions in pipelines by use of a laser device was developed in a previous study [10].

This study was conducted as a part of a project focusing on investigation of scale formation in aluminium production plants. In this paper,

the results of a test campaign in which the active acoustic method was used together with the laser imaging method to monitor scale propagation in a pneumatic conveying system is presented. The tests were performed in a Norwegian aluminium smelter where the monitoring equipment was installed in an area along a pipeline known to be particularly exposed to scaling. In the analysis of the measurements obtained during the test campaign, special emphasis was placed on detecting periods where the scaling rate had increased or decreased. Such periods would be of great interests for the continuing studies in this project. It is assumed that if periods of increased or decreased scaling rate can be found, an analysis of the prevailing ambient and process conditions during these periods can provide useful information related to the underlaying scaling mechanism. Also, the most important factors influencing scaling may be identified. Thus, the results from this paper was used in a follow up study focused on discussion of possible scale formation mechanisms [11].

2. Materials and methods

2.1. The pneumatic conveying system

In this study, a pneumatic conveying system located in a Norwegian aluminium smelter, transporting secondary alumina from a gas treatment centre (GTC) to a group of metal production cells, was considered. The pneumatic conveying system is a version of the ALESA system which is described in some detail in [12]. Consisting of a blow tank sending off batches of material which is conveyed through a pipeline ($l = 160$ m, $d = 88.9$ mm), the conveying system distributes secondary alumina to small storage silos on top of each of the metal production cells. The pipeline has several bends of various angles and both horizontal and vertical sections. The bends are of a special design referred to as "pot bends" in [12]. Dense phase conveying of secondary alumina particles is facilitated by a pipe-in-pipe design, with narrow internal air bypass pipe segments attached in the top of the main pipeline. During operation of the conveying system, a dispatched batch of material will be transported for some distance before the material falls out of suspension and clogs the pipeline. Subsequently, air will flow through the bypass lines and emerge to break the blockage into shorter plugs. The short plugs are conveyed further through the pipeline by the available pressure in the system before new blockages form and the process repeats [12]. The pneumatic conveying system is operated in four-hour cycles in which secondary alumina is filled to each of the silos on the metal production cells before the system is shut down for a shorter period awaiting start-up of the next cycle.

In the test campaign performed in the production plant, scale growth was monitored in a test area along a horizontal part of the pipeline. Located after a 90° "pot bend", the test area was situated in a zone of turbulent flow which represents a problematic spot where a lot of scale typically forms. Equivalent pipe sections have been choked by the scale in the past.

2.2. The conveyed material

Secondary alumina is formed when primary alumina (also referred to as smelter grade alumina [5]) is used to clean production off-gas in gas treatment centres. In addition to adsorbing gaseous and particulate fluoride components, the alumina also captures various impurities from the off-gas. Some of the main contaminations are P, Fe, Mn, Si, Ti, Zn, Ga, Be, Li and Mg [13]. Secondary alumina typically has a smaller mean particle size than primary alumina, partly due to attrition of the particles in the gas cleaning and transport processes and partly as a result of the fine pot gas dust, which transfers more or less unchanged into the secondary alumina during the dry scrubbing of production off-gas [13]. Typical values for some properties of secondary alumina are given in Table 1. The properties of the secondary alumina will vary in accordance with variations in primary alumina used in the gas scrubbing process, the

Table 1
Typical values of some properties for secondary alumina.

Description	Value
x_{10} [μm]	30.0
x_{50} [μm]	81.6
x_{90} [μm]	142.0
Particle density [g/cm^3]	3.497

raw gas composition and process parameters such as gas velocity and particle attrition in the dry scrubbers.

2.3. Active acoustic monitoring method

The active acoustic method is a recently developed version of acoustic chemometrics. The basic idea of the new version of acoustic chemometrics is that an acoustic signal which is sent into a system will be modified by the system in a manner influenced by various physical system properties. Thus, the frequency response output signals resulting from exiting the system by acoustic stimuli contain latent information about the system properties. In the active method, acoustic signals are sent into a system by a transducer and the output signals are measured by acoustic sensors. The measured signals are processed and transformed to produce frequency domain acoustic spectra. Multivariate analysis methods are used to extract the underlaying information from such spectra and relate it to the monitored characteristics of the system. The active acoustic method is discussed in detail in [9]. More information about acoustic chemometrics can be found in [8].

In comparison to other PAT monitoring methods, the equipment needed for acoustic chemometrics is relatively inexpensive and easy to install. Furthermore, the method is non-invasive, meaning no part of the measuring equipment needs to be placed inside the pipeline. This is essential to successfully monitor alumina scaling as scale material would otherwise quickly attach to the measuring equipment and impede the monitoring process. Also, any disturbance in the gas flow could create more turbulence in the pipeline and thus lead to more scale growth. The dense phase transportation process, with periods of choking of the pipeline and subsequent formation of plugs, could potentially induce much noise in the measurements. However, the active acoustic method is relatively robust against influence from noise and fluctuations in the monitored system. Finally, the acoustic method can provide real-time predictions of scale growth once a model relating acoustic spectra to scaling has been calibrated. Altogether, these advantages make the acoustic method suitable for monitoring of alumina scaling in pneumatic conveying systems. Nevertheless, the method is indirect and completely dependent upon the availability of reliable reference measurements to calibrate models [14] of scale growth, representing a challenge of the method.

2.4. Reference measurements by laser device

Recently, a technique was developed to solve the challenge of obtaining reliable reference measurements of scale growth in pipes [10]. In this technique, a device is used to capture images of laser light tracing an inner cross section of a pipe by slow shutter photography. Images captured by the device are pre-processed in order to isolate the laser traces before the images are analysed. Calculation of some statistical values describing the scale thickness and distribution in the pipe cross section as well as the cross-sectional area of the pipe covered by the scale are performed to quantify the scale growth.

2.5. Experimental setup and procedure

The measurement equipment was permanently installed in the test area for the duration of the test campaign. Four piezo elements (one transducer and three sensors, 7BB-20-6 L0) were glued to the surface

of the pipe section in the test area, hereafter referred to as the test pipe, in the configuration shown in Fig. 1. A function generator (Escort EGC-3230) was used to produce the acoustic input signals (square waveforms with increasing frequency (0–20 kHz) and constant amplitude). A SAM-unit (developed by the applied chemometrics research group at the University of South-Eastern Norway) amplified the measured signals before A/D conversion was performed by a DAQ-device (NI-Instruments). The data acquisition was performed by a LabVIEW (NI-Instruments) code running in a remote-controlled computer (LogMeIn Pro) stationed near the test area in the plant. Throughout the test campaign, three replicate measurements were obtained by each acoustic sensor while powder transport was ongoing during each four-hour cycle in the pneumatic conveying system. Thus, six groups of replicate measurements for each sensor were normally obtained each day of the campaign.

Images were obtained by the laser device from the spot marked in Fig. 1 a) by plant personnel on a weekly basis when possible. However, limitations in the time schedules of the operators restricted the opportunity to obtain images in some periods, especially during the summer vacation season. When the images were captured, the test pipe had to be disconnected from the main pipeline and any remaining powder had to be removed. The images where captured during the cyclic down-times of the pneumatic conveying systems.

Image processing software (GIMP 2.0) was used to pre-treat the images captured by the laser device. The images were slightly aligned and cropped to the same size before various selection tools were used to isolate the laser traces in the images. Subsequently, a MATLAB (version 9.1.0.441655, R2016b) code was used to perform calculations of scale growth based on the images. Due to the presence of the internal bypass pipe segments discussed in Section 2.1., an area of the photographed pipe cross section was blocked from the view of the camera. This area was disregarded during the image analysis, as discussed in detail in [10].

2.6. Multivariate data analysis

As acoustic spectra consist of inputs from multiple frequencies and the shape of the spectra normally depends on several different variables, they make up multivariate data [15]. Thus, multivariate data analysis techniques are needed to investigate and extract information from such measurements. Multivariate data is normally structured in a $n*p$ matrix $\mathbf{X}$ in preparation for the data analysis. The rows and columns in $\mathbf{X}$ are usually referred to as objects and variables, respectively. When analysing acoustic spectra, every row in $\mathbf{X}$ contains an acoustic spectrum and every column corresponds to a certain frequency in the spectra. Various pre-processing techniques are often carried out on the data in $\mathbf{X}$ prior to the data analysis in order to remove disturbing effects and convert the data into a suitable form [14]. Mean centring and variance scaling of the columns in $\mathbf{X}$ are commonly used pre-processing techniques when analysing acoustic spectra [16].

2.6.1. Principal component analysis

Principal component analysis (PCA) is the standard technique of choice for performing exploratory analysis of a dataset and for obtaining an overview of the main structures and systematic variations in the data. In PCA, a matrix $\mathbf{X}$ is decomposed into a principal components, each represented by two vectors $\mathbf{t}$ and $\mathbf{p}$, and a matrix $\mathbf{E}$, as described in Eq. (1). The vectors $\mathbf{t}$ and $\mathbf{p}$ are called the score and loading vector, respectively. For each principal component, the loading vector defines the relationship between the component and the variables in $\mathbf{X}$ and the score vector specifies the location of each object relative to the
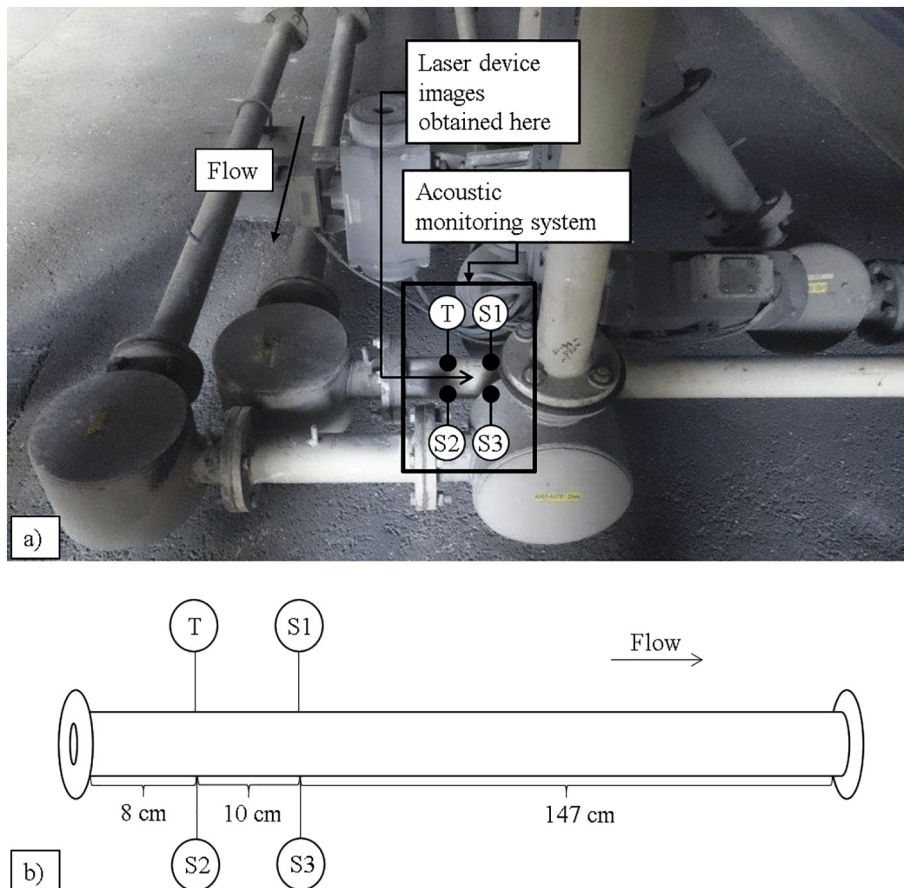

Fig. 1. A picture (a) and a schematic overview (b) of the test area and measurement setup, where T stands for a transducer and S1, S2 and S3 for three sensors.

component. The **E** matrix contains the residuals: the remaining variation from **X** which is not explained by the principal components [14].

$$X = t_1 p_1^T + t_2 p_2^T + \ldots + t_a p_a^T + E \tag{1}$$

The matrix decomposition is essentially a division of the data into an "information" part (the a principal components) and a "noise" part (the residual matrix **E**). Calculation of the principal components is done by a maximum variance criterion. Thus, the first principal component will always lie in the direction of maximum variance in the dataset. The second principal component explains the maximum variance in the remaining data after removal of the first component. The resulting components are mutually orthogonal. By this manner, up to A principal components can be calculated, where A is the mathematical rank of the **X** matrix [14]. However, normally only a few components are needed to describe the main trends in the data [15], particularly $a << A$. Thus, PCA provides a substantial reduction of dimensionality from the n columns of the matrix **X** to a small set of components, without significant loss of information in the process. Focusing on only a few components greatly simplifies the analysis of the data. The information contained in the principal components is normally investigated using various plots to visualize the data. One of the most commonly used type of plots is the score plot. A score plot is a scatter plot of the score vectors of two different principal components, and can reveal trends, groupings and outliers in the data. Outliers are measurements that differ from the majority of the data in some way [14]. If an outlier results from a faulty measurement or a failure during the data acquisition process, it should be removed from the dataset prior to further analysis of the data.

2.6.2. Partial least squares regression

Whereas PCA considers the internal variation in the **X** matrix, partial least squares regression (PLS-R) establishes how this matrix relates to a response vector **y**. PLS-R also involves matrix decomposition as described in Eq. (1), but in this case, it is a criterium of maximum correlation between **X** and **y** which guides the decomposition. Thus, the components obtained by the PLS-R method are different from the principal components found in PCA. The "information" part of **X** extracted in the PLS-R matrix decomposition is connected to the relation between **X** and **y**. This information is used to calibrate a linear model describing the relationship between **X** (independent variables) and **y** (dependent variable) based on the data in a calibration data set containing measured **X** data and corresponding **y** values [15].

Various plots providing geometrical representations of the data are normally used to simplify interpretation and aid in the model calibration. For example, t-u scatter plots show the "inner relation" between **X** and **y** and are typically inspected to search for outliers. Furthermore, the number of components to include in the model can be decided by finding the first minimum value in a residual validation variance plot [14]. Numerous other plots are also available and can be used as needed.

In order to evaluate how well the calibrated model will be able to predict future values of **y** based on future **X** measurements, it must be validated against a test set containing new, independent measurements of **X** and **y** [17]. In test set validation, the calibrated model is used to predict values of **y** based on input **X** measurements. The reliability of the model's predictions can be assessed based on inspection of a scatter plot of predicted versus measured values of **y** and calculation of some diagnostic statistics; the slope, offset and correlation coefficient (r^2) of a linear curve fitted to the points in the scatter plot. Additionally, the root mean squares error of prediction (RMSEP) can be calculated by comparing the predicted values of **y** with the measured values contained in the validation dataset as described in Eq. (2). The RMSEP value has the same unit as **y** and gives an estimation of the error associated with future predictions by the calibration model [14].

$$RMSEP = \sqrt{\frac{\sum_{i=1}^{n} \left(\hat{y}_{i,predicted} - y_{i,reference} \right)^2}{n}} \tag{2}$$

Unscrambler version 10.3 (Camo Software AS, Norway) and MATLAB (version 9.1.0.441655, R2016b) was used to perform the data analysis.

3. Results and discussion

3.1. Images obtained by the laser device

A total of 13 images were captured by the laser device throughout the plant test campaign. When analysing these images, it was found that the positions of the laser traces sometimes shifted slightly relative to each other from one picture to the next. This shows that it was not possible to place the laser device in the exact same position in the pipe every time an image was captured. To counteract the uneven positioning of the laser device, some of the images were aligned to obtain the best fit of the laser traces. The further analysis of the images and the measured data was based solely on the calculations of area blocked by the scale, as this property should not be affected by the alignment of the images and thus is more reliable than the statistical properties described in [10]. Based on the estimated values for the area of the pipe blocked by scale, a mean scale thickness value was also calculated for each image. The mean scale thickness value contributes to concretize the scale build-up in the pipe, but it should be kept in mind that the scale considered in this study does not deposit in even layers.

Table 2 lists the calculated values describing the area of the test pipe cross section which was covered by scale as well as the mean scale thickness based on each of the images obtained in this study. A part of the pipe cross section was disregarded during calculations of the values in Table 2 as discussed in Section 2.5 and in [10]. Thus, the values in Table 2 describe only the scale growth in the area considered when analysing the images.

Some of the images of the scale in the test pipe obtained by the laser device are shown in Fig. 2. Table 2 and Fig. 2 show that the laser imaging method has been capable of documenting the growth of scale in the pipe over time. The images captured by the laser device also describe the distribution of the scale over the pipe cross section during the test campaign. In general, the scale grew mostly on the side walls of the pipe and less in the bottom of the pipe. At the start of the test campaign, some scale had already deposited on the left wall of the test pipe section, consecutive to the inner wall of the upstream pot bend. Scaling continued mainly in this region for some time before significant depositions

Table 2
Calculated values quantifying the scale growth in the test pipe during the measurement campaign.

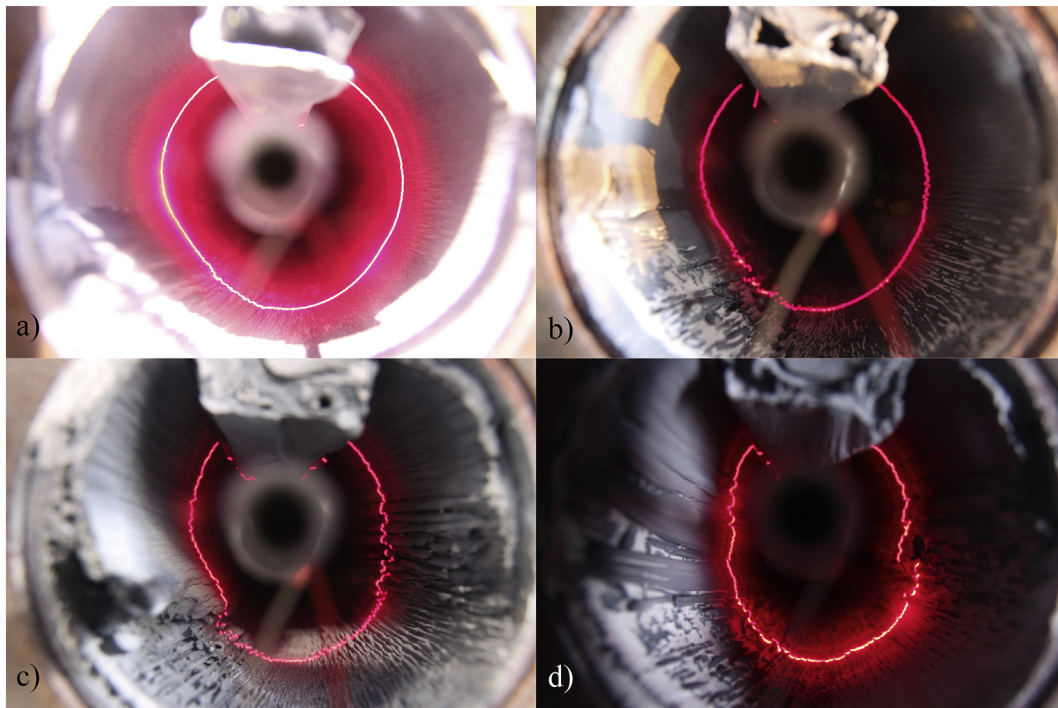| Date	Area [cm2]	Area [%]	Mean thickness [mm]
2/21/2017	0.4	1.0	0.2
4/26/2017	3.0	7.1	1.5
5/3/2017	3.4	8.1	1.7
5/11/2017	3.2	7.6	1.6
5/19/2017	3.4	8.1	1.7
5/30/2017	5.3	12.6	2.7
6/9/2017	5.3	12.6	2.7
6/16/2017	5.6	13.3	2.9
8/24/2017	9.7	23.1	5.1
9/1/2017	10.0	23.8	5.2
9/15/2017	11.0	26.2	5.8
10/19/2017	12.3	29.3	6.6
11/22/2017	11.6	27.6	6.2

Fig. 2. Some of the images of the scale in the test pipe obtained in the test campaign. a) 21.02.17, b) 19.05.17, c) 24.08.17, d) 22.11.17.

started to form on the right pipe wall following the outer wall of the upstream pot bend. The images do not provide sufficient information to describe scale growth in the top of the pipe because of the inner pipe section blocking the view in this area. However, it can be seen from visual inspection of the images that the inner pipe segment in the top of the pipe is gradually chocked by the scale. These observations are only valid for the specific position where the images where captured and for the specific time period when the test campaign was conducted. Scale formation could develop in a different manner in similar positions in the pipeline and even in the same location at a different time period. In order to make any general conclusions on the distribution of the scale after a pot bend, further tests from several different locations are needed.

From visual inspection of the images, wear patterns in the form of grooves in the scale in the direction of the gas flow, as described in [4], can be seen. The depth of these grooves seems to increase with time. Also, several occurrences of lumps of scale forming and later disappearing were found. The most noticeable example is a lump of scale that gradually formed in the left lower region of the test pipe (Fig. 2 c). In Fig. 2 d), the lump has disappeared and a smooth surface is left where it used to be located. This could be a result of erosion by the conveyed powder, mechanical chip off of the scale pieces, or a combination of both. The test pipe had to be detached from the pipeline every time an image was obtained, and it is plausible that pieces of scale broke off when this was done, especially if scale had grown across the pipe flanges joining the test pipe to the main pipeline.

3.2. Estimation of scale growth curve based on images

A curve was fitted to the values calculated from the images obtained by the laser device (Table 2) using the curve fitting tool in MATLAB (smoothed spline method). Fig. 3 shows a plot of the resulting scale growth curve, the calculated values of the area of pipe cross section blocked by scale (Table 2) and the associated pre-treated images for each calculated value. The scale growth curve was re-sampled to get one value per day, providing estimations of the scale progression throughout the test campaign.

3.3. Development of acoustic chemometrics models of scale growth

The analysis of the data measured by the acoustic sensors was conducted in two separate steps. First PCA was used to perform an exploratory analysis of the data, then calibration of PLS-R models of scale growth based on a portion of the data selected in step one was conducted. All variables were mean centred and scaled to unit variance prior to the data analysis.

3.3.1. Step 1: exploratory data analysis

PCA was performed on a dataset containing all the acoustic measurements obtained during the test campaign in order to get an overview of the main data structures and look for groupings and outliers in the data. Score plots for the first component plotted against the second and third component, respectively, is shown in Fig. 4. The plots in Fig. 4 are based on data from sensor 1 (S1 in Fig. 1).

Several groupings of measurements can be seen in the plots in Fig. 4, some groups can be found in both plots and some are only distinct in one of the plots. The measurements in each of these groups were investigated further to uncover why they differ from the main group. It was found that a cable had detached from the sensor before the measurements in group 1 were obtained, explaining their deviating positions in the score plots. The measurements in group 2 were obtained during the initiation of the test campaign in periods of temporary shutdown of the pneumatic conveying system from which the measurements were acquired. Unsurprisingly, these measurements differ substantially from measurements obtained while powder was transported through the pipeline. During down-time of the pneumatic conveying system, varying amounts of powder would be present in the bottom of the test pipe. As the variations in powder content in the test pipe during downtimes would create a lot of noise in the measurements, it was decided to conduct measurements only while powder transport was ongoing for the remainder of the test campaign. No clear reasons were found explaining why the measurement in group 3 is positioned away from the main group, but the deviation is significant. The measurements in group 1, 2 and 3 were all considered as outliers, and they were removed from the dataset before proceeding to step 2 of the data analysis.
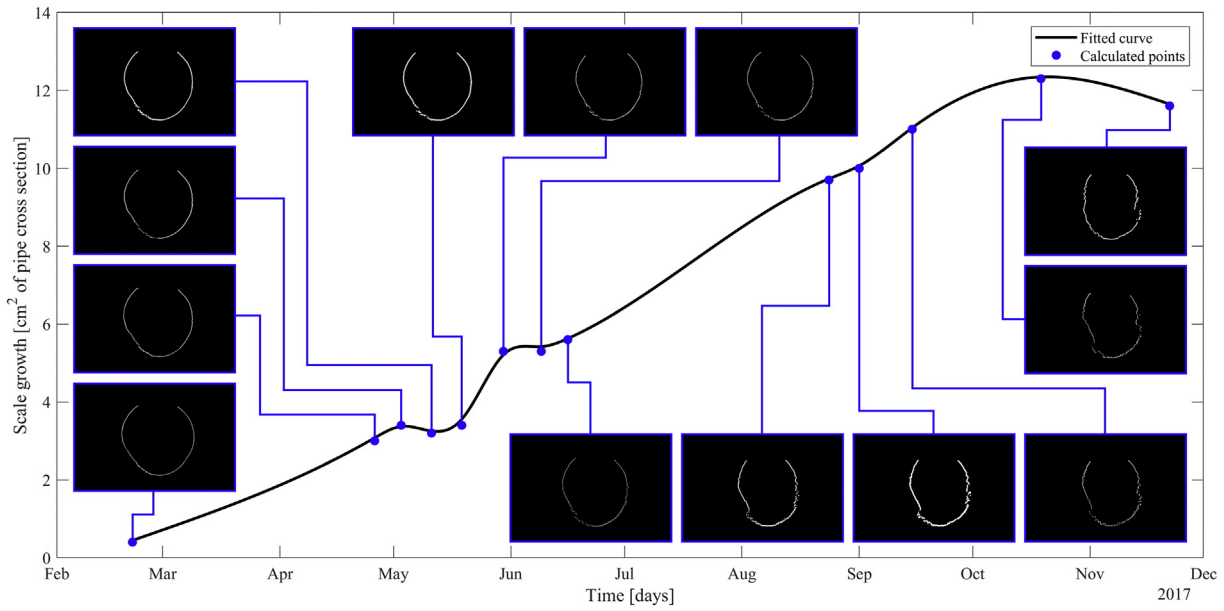
Fig. 3. Scale growth curve fitted by smoothing spline based on calculated values from the images obtained by the laser device.

There was a temporary break in the acoustic monitoring of the scale growth for a period during the test campaign (mid-April to mid-May 2017) as some of the equipment used for obtaining the measurements accidentally shut down. The measurements in group 4 were obtained prior to this disruption. Only the measurements from the period after the breakdown (mid-May to mid-October 2017), located in group 5 in Fig. 4, were included in the development of the models in step 2. For these data, mean values of all measurements from each day were calculated to create a dataset with one acoustic spectrum per sensor for each day of the test campaign.
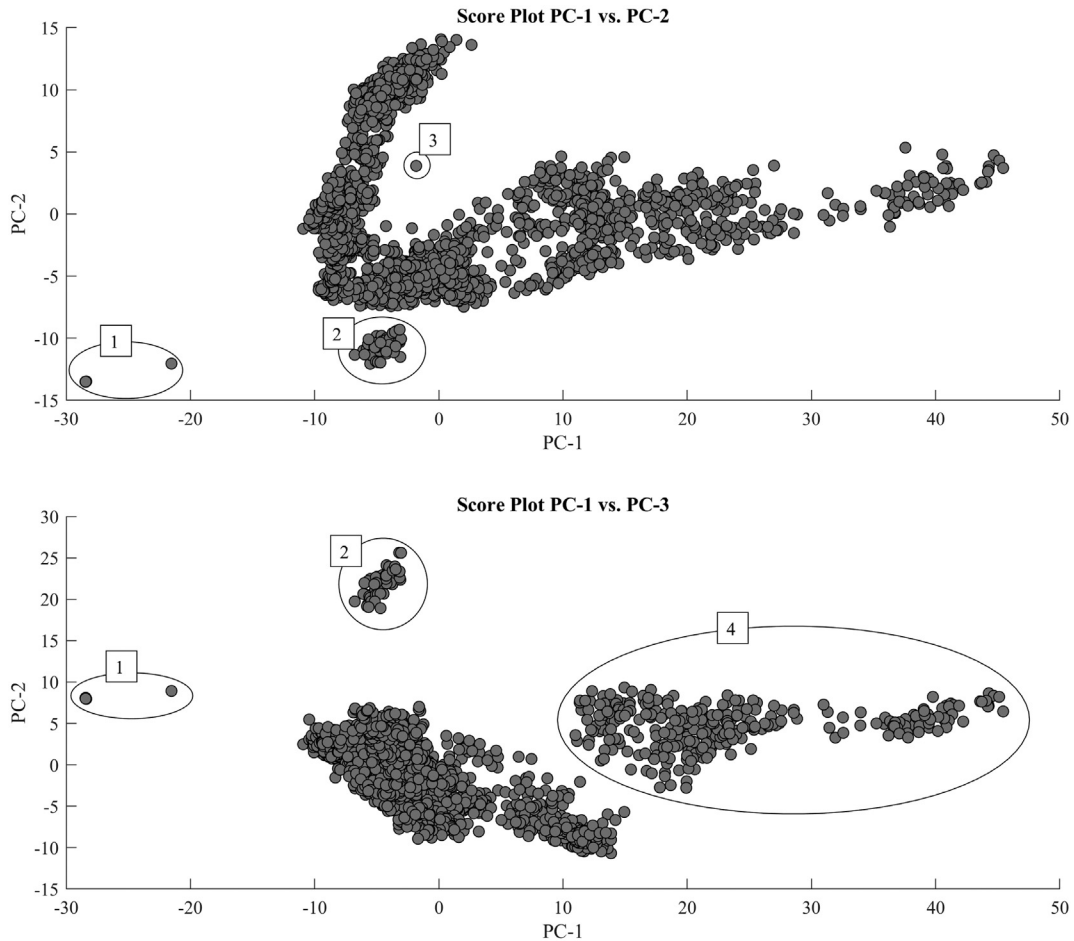

Fig. 4. Score plot for PC-1 vs PC-2 and PC-1 vs PC-3, respectively.

Similar plots as the ones shown in Fig. 4 were also created based on data from sensor 2 and sensor 3 (S2 and S3 in Fig. 1), and comparable groupings were found in the analysis of these plots.

3.3.2. Step 2: development of calibration models

Every other measurement obtained during the test campaign were assigned to a calibration set and a validation set, respectively. PLS-R models were calibrated using the measurements from sensor 1 and sensor 2 as independent variables and the estimated values for scale growth calculated in Section 3.2 as the dependent variable. Plots describing the calibration results of the models based on data from sensor 1 and 2 are shown in Fig. 5 and Fig. 6, respectively. No model was calibrated based on the data from sensor 3 as there were too few measurements available; the sensor had accidentally been ripped off the test pipe in the middle of the test campaign.

A few measurements are located somewhat far away from the straight regression lines in the X-y Relation Outlier plots (t-u plots) in Fig. 5 and Fig. 6. These measurements constitute outlier candidates. However, the deviations of these points are not major, and a closer investigation of the measurements did not reveal any specific reason explaining why they differ from the other points. Thus, it was assumed that the outlier candidates were correctly obtained measurements representing unusual conditions in the pneumatic conveying system, and they were not removed from the dataset.

The selection of the number of components to include in each of the models were done by inspection of the Residual Variation Variance plots in Fig. 5 and Fig. 6. Three components were used in each model.

The Predicted vs. Reference plots in Figs. 5 and 6 and the corresponding model statistics confirm that the PLS-R models based on acoustic measurements from sensor 1 and 2 have been successful in describing the scale growth in the test pipe in detail. However, the validation technique used in the study does not constitute a complete test set validation as a new and independent test set would be required for this and such a test set was not available. Thus, no conclusion can be made concerning how well the method would be able to predict new response values in real-time given new and independent acoustic measurements at this stage. Further tests are needed to investigate this matter.

The scale growth predicted by the PLS-R models was compared to the scale growth curve derived from the images obtained by the laser device in the Predicted and Reference plots in Figs. 5 and 6. These plots reveal a very good agreement between the scale growth curves obtained by the two different methods. Furthermore, it is apparent that the scale growth curve predicted based on acoustic model might contain more information about the scale progression during the test period, indicating periods where the scale growth has intensified or decreased and periods where a piece of scale seems to have been removed from the pipe wall. Examples of the latter were also seen during the
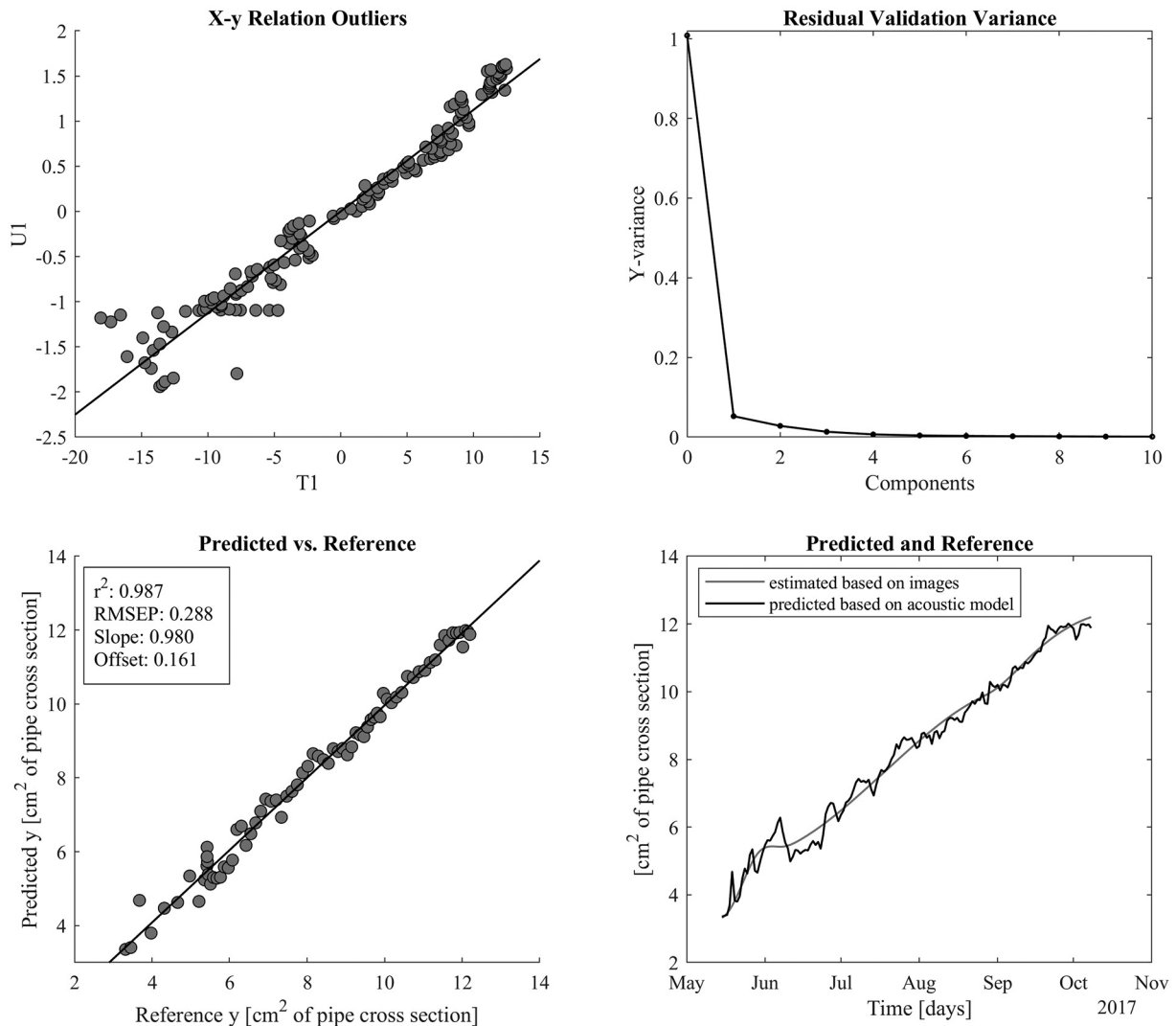

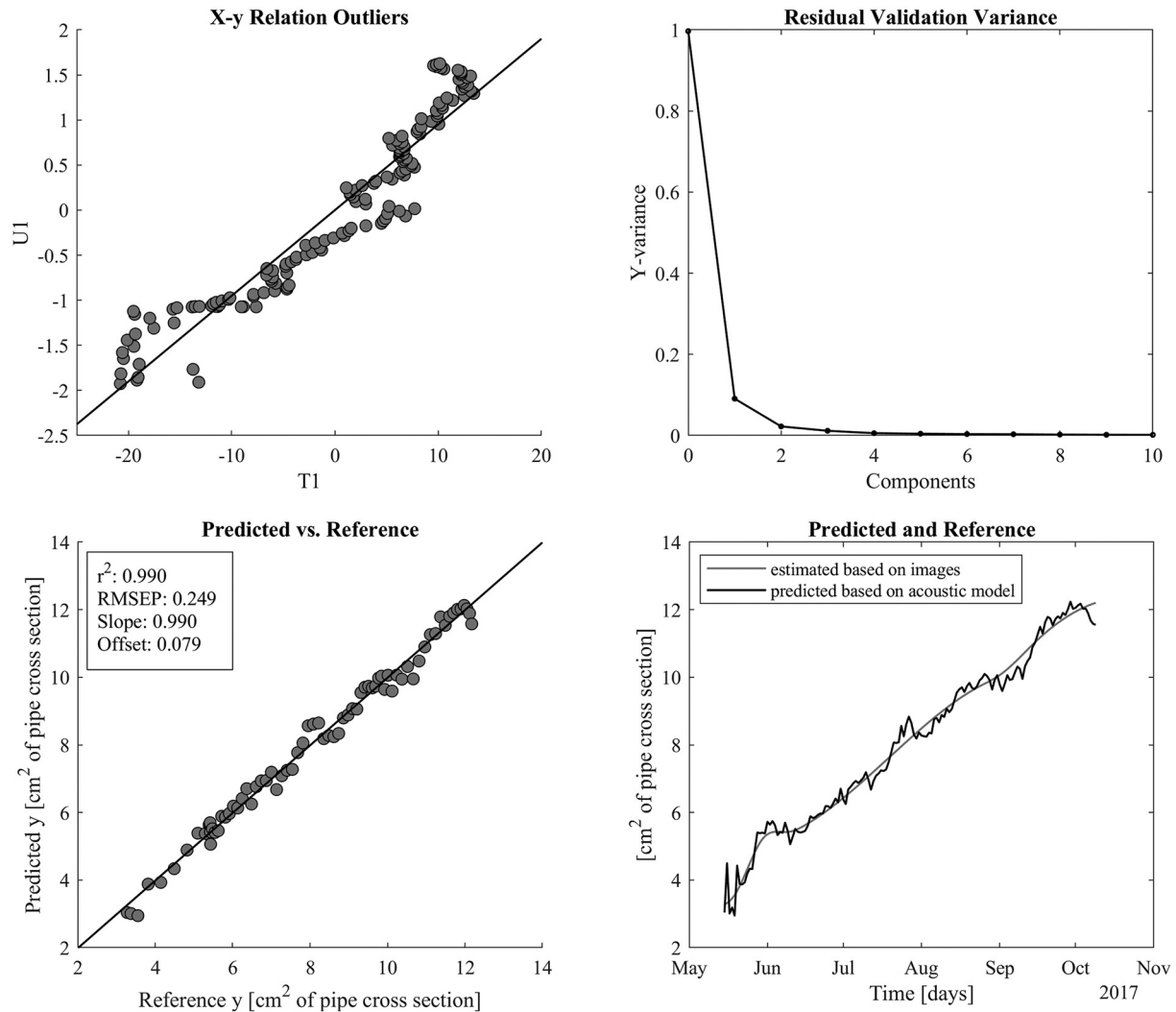**Fig. 5.** PLS calibration results for sensor 1.

Fig. 6. PLS calibration results for sensor 2.

analysis of the images captured using the laser device, as discussed in Section 3.1. The curve describing the predicted scale growth based on sensor 1 in Fig. 5 is fluctuating with high amplitudes in the beginning of the modelled period. The amplitudes of the fluctuations decrease with time. Most likely, this is an effect of the system becoming more stiff and robust and less prone to vibration induced by the transducer as the amount of scale in the pipe increase. As a result, the acoustic response measured by sensor 1 decrease. The corresponding curve based on measurements from sensor 2, shown in Fig. 6, did not follow the same trend; no systematic change was found in the amplitude of the fluctuations in this case. Sensor 2 was placed on the bottom of the pipe (Fig. 1), where the acoustic response would generally be lower than for sensor 1, which was placed on the top of the pipe (Fig. 1), due to the dense phase conveying of powder through the pipeline. Large amounts of powder conveyed primarily along the bottom of the pipeline is the cause of this effect.
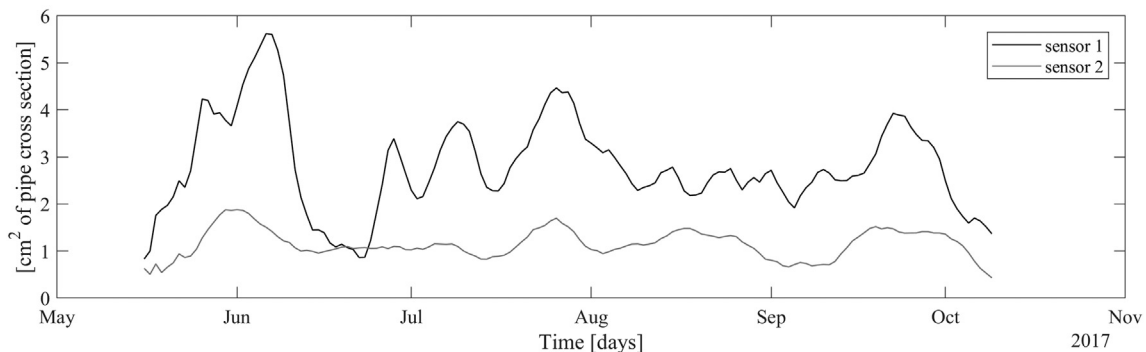

Fig. 7. A plot of the scale growth curves based on the acoustic measurements from sensor 1 and sensor 2 after detrending and smoothing.

3.4. Further processing of the scale growth curve

In order to highlight the main changes in the scale growth for the test period covered by the models (i.e., from mid-May to mid-October 2017), further processing of the predicted scale growth curves based on the acoustic measurements was performed. Linear detrending of the curves followed by smoothing by moving average (window size 5) was conducted to remove the generally increasing time trend and focus on the sub trends consisting of changes in the scaling rate. The processed curves are plotted in Fig. 7.

As can be seen in the plots in Fig. 7, the main trends in the two curves are coinciding. The curve based on measurements from sensor 1 seems to have a higher resolution and contain more detailed information about the scale growth than the corresponding curve for sensor 2. As discussed in Section 3.3.2, the most likely reason for this is that the conveying of powder along the bottom of the pipe during measurements has resulted in lower acoustic responses for sensor 2. During the test campaign, various process and other data was collected. In a follow-up study, the scale growth curve based on sensor 1 measurements was compared with variations in the data collected in the same test period to identify variables and process conditions which could influence scaling [11].

4. Conclusions

This paper demonstrates how the active acoustic method can be combined with a laser imaging method to monitor scaling in pneumatic conveying systems. The results from a five-month long monitoring period in which the two methods have been applied is presented, providing the first ever in-depth study of scale progression in an aluminium production plant.

The laser device used in this study was at a prototype stage, and the results showed that constant positioning of the device in the test pipe has not been possible when obtaining images during the test campaign. Thus, efforts should be made to improve the precision of the device's positioning function and make the design more robust and stable for future applications of the method. Nevertheless, the laser device was successful in providing reliable reference measurements of the scale thickness by calculation of the cross-sectional pipe area blocked by the scale from the images. Additionally, visual inspection of the images offered information about the spatial distribution of the scale growth in the pipe cross section.

Calibration results indicate that the acoustic method has been able to capture the scale growth in a reliable manner. Models calibrated based on each of the two sensors showed the same main trends in scale progression for the monitoring period. Prediction results from the calibrated models demonstrated that the scale is generally growing relatively steadily during the measuring campaign. Some periods of increasing or decreasing scale growth rate as well as periods where scale seemed to have been removed from the pipe surface were found. These trends were highlighted by detrending and smoothing of the scaling curves. The scale growth curves obtained in this study were compared with data collected during the same test period to investigate which variables and process parameters could have influence on the scale formation in a follow-up study [11].

Nomenclature

A	Maximum number of components that can be extracted from **X**
a	Number of components extracted from **X**
Calibration set	Dataset containing measurements of **X** and corresponding measurements of **y**, used to calibrate models
E	Matrix containing **X**-residuals
GTC	Gas treatment centre
HGS	Hard grey scale
Offset	Offset of the regression curve in a predicted vs. measured plot
Outlier	Deviating measurement
n	Number of rows in **X** and **y**
p	Number of columns in **X**
p	Loading vector
PAT	Process analytical technology
PCA	Principal component analysis
PLS-R	Partial least squares regression
r^2	Squared correlation coefficient
RMSEP	Root mean square error of prediction
Secondary alumina	Alumina which has been used for dry scrubbing of process off-gas
Slope	Slope of the regression curve in a predicted vs. measured plot
t	Score vector
Validation set	Dataset containing measurements of **X** and corresponding measurements of **y**, used to validate models
X	Multivariate data matrix, independent variables in calibration
y	Response variable, dependent variable in calibration

References

[1] G.E. Klinzing, F. Rizk, R. Marcus, L.S. Leung, in: B. Scarlett, G. Jimbo (Eds.), Pneumatic Conveying of Solids, Chapman & Hall, London, 1997.

[2] A. Rawat, H. Kalman, Detachment velocity: a borderline between different types of particulate plugs, Powder Technol. 321 (2017) 293–300.

[3] G.E. Klinzing, A review of pneumatic conveying status, advances and projections, Powder Technol. 333 (2018) 78–90.

[4] N.R. Dando, S.J. Lindsay, Hard gray scale, in: G. Bearne, M. Dupuis, G. Tarcy (Eds.), Essential Readings in Light Metals, Aluminum Reduction Technology, Wiley, Hoboken 2013, pp. 602–607.

[5] S.J. Lindsay, N.R. Dando, Dry scrubbing for modern pre-bake cells, in: G. Bearne, M. Dupuis, G. Tarcy (Eds.), Essential Readings in Light Metals, Aluminum Reduction Technology, Wiley, Hoboken 2013, pp. 981–986.

[6] H. Gaertner, A.P. Ratvik, T.A. Aarhaug, Raw gas particles and depositions in fume treatment facilities in aluminium smelting, in: J. Grandfield (Ed.), Light Metals 2014, Wiley, Hoboken 2014, pp. 547–552.

[7] L.L. Simon, H. Pataki, G. Marosi, F. Meemken, K. Hungerbühler, A. Baiker, S. Tummala, B. Glennon, M. Kuentz, G. Steele, H.J.M. Kramer, J.W. Rydzak, Z. Chen, J. Morris, F. Kjell, R. Singh, R. Gani, K.V. Gernaey, M. Louhi-Kultanen, J. O'Reilly, N. Sandler, O. Antikainen, J. Yliruusi, P. Frohberg, J. Ulrich, R.D. Braatz, T. Leyssens, M. von Stosch, R. Oliveira, R.B.H. Tan, H. Wu, M. Khan, D. O'Grady, A. Pandey, R. Westra, E. Delle-Case, D. Pape, D. Angelosante, Y. Maret, O. Steiger, M. Lenner, K. Abbou-Oucherif, Z.K. Nagy, J.D. Litster, V.K. Kamaraju, M.-S. Chiu, Assessment of recent process analytical technology (PAT) trends: a multiauthor review, Org. Process. Res. Dev. 19 (2015) 3–62.

[8] M. Halstensen, K.H. Esbensen, Acoustic chemometric monitoring of industrial production processes, in: K. Bakeev (Ed.), Process Analytical Technology, Wiley-Blackwell, Oxford 2010, pp. 281–302.

[9] I.B. Haugland, M. Halstensen, Online acoustic chemometrics monitoring of scale deposition thickness in pneumatic conveying systems: a feasibility study, in: C. Ratnayake (Ed.), The 5th International Symposium of Relpowflo, 2017 , Skien, Norway.

[10] I.B. Haugland, M. Halstensen, A technique for obtaining reference measurements to calibrate deposition models for pipelines, Chem. Eng. Technol. 41 (2018) 1538–1543.

[11] I.B. Haugland, O. Kjos, A. Røyset, P.E. Vullum, T.A. Aarhaug, M. Halstensen, Alumina scale composition and growth rate in distribution pipes, in: C. Chesonis (Ed.), Light Metals 2019, The Minerals, Metals & Materials Society, Springer Nature Switzerland AG, Switzerland 2019, pp. 697–706.

[12] C. Burne, M. Bradley, Pneumatic conveying of abrasive bulk solids at Anglesey aluminium metals limited: four case studies, Proc. Instn. Mech. Eng. E. 214 (2000) 233–243.

[13] S. Kalyavina, A.P. Ratvik, T.A. Aarhaug, Impurities in raw gas and secondary alumina, in: B. Sadler (Ed.), Light metals 2013, Wiley, Hoboken 2013, pp. 195–200.

[14] K.H. Esbensen, Multivariate Data Analysis - in Practice: An Introduction to Multivariate Data Analysis and Experimental Design, 5th ed., 2001 Camo, Oslo.

[15] H. Martens, T. Næs, Multivariate Calibration, Wiley, Chichester, 1989.

[16] F.N. Ihunegbo, C. Ratnayake, M. Halstensen, Acoustic chemometrics for on-line monitoring and end-point determination of fluidised bed drying, Powder Technol. 247 (2013) 69–75.

[17] K.H. Esbensen, P. Geladi, Principles of proper validation: use and abuse of re-sampling for validation, J. Chemom. 24 (2010) 168–187.